YAP inhibits NF-κB signaling and ccRCC growth by opposing p65-ZHX2 cooperativity

Xu Li[1, 2,Ψ, #], Yong Suc Cho[1, #], Yuchen Liu[3, 4, 5], Yingzi Yang[3, 4, 5], , Shu Zhuo[1, &] and Jin Jiang[1,6*]

[1]Department of Molecular Biology, University of Texas Southwestern Medical Center, Dallas, TX 75390, USA

[2]Department of Genetics, School of Life Science, Anhui Medical University, Hefei, Anhui, China. 230032

[3]Department of Developmental Biology, Harvard School of Dental Medicine, [4]Harvard Stem Cell Institute, [5]Dana-Farber/Harvard Cancer Center, 188 Longwood Ave. Boston, MA 02215, USA

[6]Department of Pharmacology, University of Texas Southwestern Medical Center, Dallas, TX 75390, USA

[#]These authors contribute equally

[Ψ]Current address: Department of Genetics, School of Life Science, Anhui Medical University, Hefei, Anhui, China. 230032

[&]Current address: Signet Therapeutics Inc, Research Institute of Tsinghua University in Shenzhen, Shenzhen, Guangdong 518017, P.R. China.

*Corresponding authors: jin.jiang@utsouthwestern.edu

Key words: Hippo, YAP, TEAD, NF-κB, p65, ZHX2, ccRCC, cancer

Abstract

Hippo pathway functions as a tumor suppressor pathway by inhibiting the oncogenic potential of pathway effectors YAP/TAZ. However, YAP can also function as a context-dependent tumor suppressor in several types of cancer including clear cell renal cell carcinomas (ccRCC). Here we show that YAP blocks NF-κB signaling in ccRCC to inhibit cancer cell growth. Mechanistically, YAP inhibits the expression of ZHX2, a critical p65 co-factor in ccRCC. Furthermore, YAP competes with ZHX2 for binding to p65. Consequently, elevated nuclear YAP blocks the cooperativity between ZHX2 and p65, leading to diminished NF-κB target gene expression. Pharmacological inhibition of Hippo/MST1/2 blocked NF-κB transcriptional program and suppressed ccRCC cancer cell growth, which can be rescued by ZHX2/p65 overexpression. Our study uncovers a novel crosstalk between the Hippo and NF-κB pathways and its involvement in ccRCC growth inhibition, suggesting that targeting the Hippo pathway may provide a therapeutical opportunity for ccRCC treatment.

Introduction

Initially discovered in *Drosophila*, the Hippo tumor suppressor pathway is an evolutionarily conserved signaling pathway that controls organ size, tissue homeostasis, and cancer progression among different species[1-3]. The Hippo pathway consists of a core kinase cascade with upstream kinases Hippo (Hpo)/MST1/2 phosphorylating and activating downstream kinases LATS1/2 [4-8], resulting in phosphorylation of the transcriptional effector proteins YAP/TAZ, which inhibits YAP/TAZ activity by restricting their nuclear translocation[9-11]. When the activity of Hippo kinase cascade is compromised, unphosphorylated YAP/TAZ translocates into the nucleus, forms a complex with the TEAD-family of transcription factors, and activates Hippo pathway target genes[11-13]. Aberrant activation of YAP due to mutation in upstream components, gene amplification or fusion, or other mechanisms promotes tumor progression in many types of cancer including Hepatocellular carcinoma, lung adenocarcinoma, gastric cancer, colon cancer, mesothelioma, schwannomas, ependymomas, cervical squamous cell carcinoma, uveal melanomas, and esophageal squamous cell carcinoma[2,3,14]. Consistent with these clinical observations, transgenic overexpression of YAP or knockout of upstream Hippo pathway components in mouse livers resulted in hepatomegaly, leading to hepatocellular carcinoma formation[10,15-20]. Taken together, these studies have led to a prevalent view that Hippo signaling functions as a tumor suppressor pathway by blocking the oncogenic potential of YAP/TAZ. However, recent studies have revealed that YAP can function as a context-dependent tumor suppressor in several types of cancer including hematological cancers[21], estrogen receptor α (ERα) positive breast cancer[22,23,24], androgen receptor (AR) positive prostate cancer[25], and VHL negative clear cell renal cell carcinoma (ccRCC)[26].

ccRCC makes up ~80% of kidney cancer, which is among the top ten most diagnosed cancers around the world[27]. ccRCC is responsible for most of the kidney cancer-associated death[28]. The majority cases of ccRCC (>90%) resulted from loss-of-function the *Von Hippel-*

Lindau (*VHL*) tumor suppressor gene, leading to stabilization and activation of Hypoxia-inducible factor 2α (HIF-2α) transcriptional program[29]. In addition to regulating HIF-2α, the VHL E3 ubiquitin ligase has other substrates that may also play important role in the progression of ccRCC because ccRCC patient samples exhibited differential sensitivity to HIF-2α inhibitors[30-32]. A genome-wide *in vitro* expression strategy identified Zinc fingers and homeoboxes 2 (ZHX2) as a VHL substrate[33]. ZHX2 plays a pivotal role in ccRCC progression by activating the nuclear factor κB (NF-κB) pathway via interacting with the p65 subunit of NF-κB[33].

Our previous study revealed that inhibition of Hippo signaling pathway or transgenic activation of YAP blocked the HIF2 transcriptional program and ccRCC tumor growth[26]. Here, we showed that YAP activation also inhibited NF-κB pathway in addition to HIF-2. Mechanistically, YAP acts in conjunction with TEAD to inhibit the expression of ZHX2 and its ability to bind p65, thereby blocking the cooperativity between ZHX2 and p65 required for NF-κB target gene expression and ccRCC growth. Pharmacological inhibition of Hippo/MST1/2 kinase activity inhibited p65/ZHX2 cooperativity, leading to diminished NF-κB target gene expression and inhibited ccRCC tumor growth, which can be alleviated by increasing the activity of ZHX2 or p65.

Results

YAP activation inhibits ccRCC cancer cell growth in 2D cultures

We have previously shown that activation of YAP, either by treatment with a small molecule inhibitor of Hippo/MST1/2 kinase XMU-MP-1[34], or by overexpression of a constitutively active YAP (YAP-5SA)[9], inhibited ccRCC cell growth in both 3D cultures and Xenografts[26]. Consistent with growth inhibition, both XMU-MP-1 and YAP5SA inhibit HIF-2 pathway activity, which is required for ccRCC cell growth in both 3D cultures and mice. Intriguingly, we found that XMU-MP-1 also inhibited cell growth in 2D cultures of multiple VHL mutant ccRCC cell lines including 786-O cells where HIF-2 pathway activity was dispensable for their growth (Fig. 1a-c) [31,35,36], raising the possibility that XMU-MP-1 could inhibit ccRCC cell growth through a mechanism(s) other than blocking HIF-2 pathway activity.

To determine whether XMU-MP-1 inhibited ccRCC cell growth in 2D cultures through the Hippo pathway instead of an off-target effect, we generated Flag (Fg)-tagged wild type (Fg-MST2^{WT}) and a mutant form of MST2 carrying Y101D and D109A double mutations (Fg-MST2$^{Y101D/D109A}$). It has been demonstrated previously that MST2$^{Y101D/D109A}$ exhibited normal kinase activity; however, it no longer binds XMU-MP-1 and thus is insensitive to drug inhibition[34]. As expected, expression of either Fg-MST2^{WT} or Fg-MST2$^{Y101D/D109A}$ increased the cytoplasmic level while decreased the nuclear level of YAP in 786-O cells, suggesting that exogenously expressed MST2 could increase the phosphorylation of YAP, leading to its cytoplasmic retention (Fig. 1d). Expression of either Fg-MST2^{WT} or Fg-MST2$^{Y101D/D109A}$ in 786-O cells slightly increased cell growth (Fig. 1e); However, only Fg-MST2$^{Y101D/D109A}$ significantly rescued XMU-MP-1-mediated growth inhibition (Fig. 1f). Hence, XMU-MP-1 inhibited 786-O cell growth mainly through an on-target effect, i.e., by inhibiting MST1/2 kinase activity to increase YAP nuclear localization.

To further investigate how perturbation of Hippo signaling affects ccRCC cell growth in 2D culture, we treated 786-O cells with different doses of XMU-MP-1 and found that XMU-MP-1 inhibited 786-O cell growth in a dose dependent manner (Fig. 1g). Furthermore, infection of 786-O cells with lentivirus expressing either the constitutively active YAP (YAP-5SA) or TAZ (TAZ-4SA) resulted in significant growth inhibition (Fig. 1h-i). To determine whether XMU-MP-1 inhibited ccRCC cell growth depending on the status of VHL, we introduced VHL back into 786-O to generate 786-O-VHL cell lines. Compared with original 786-O cell line or a control 786-O cell line expressing the empty vector (786-O-Vector), 786-O-VHL cells are less sensitive to XMU-MP-1-mediated growth inhibition (Fig. 1j-l), suggesting that XMU-MP-1 may act through another VHL target(s) to inhibit 786-O cell growth in 2D cultures.

YAP activation inhibits the transcriptional program of NF-κB in ccRCC

A previous study identified ZHX2 as a VHL target upregulated in VHL mutant ccRCC tumors and showed that ZHX2 is essential for VHL mutant ccRCC cell growth *in vitro* and in *vivo*[33]. Furthermore, this study demonstrated that ZHX2 promoted ccRCC tumor growth by promoting NF-κB pathway activity.

To determine whether XMU-MP-1 could inhibit ccRCC through the NF-κB pathway, we carried out RNAseq experiments of 786-O cells treated with XMU-MP-1 or vehicle. Gene Ontology (GO) enrichment analysis of differentially expressed genes revealed that NF-κB signaling is among the top downregulated pathways in addition of HIF (Hypoxia) pathway (Fig.2a). Gene Set Enrichment Analysis (GSEA) revealed an enrichment of NF-κB pathway genes that were downregulated by XMU-MP-1(Fig. 2b). Further analysis of the RNAseq data indicated that XMU-MP-1 downregulated many NF-κB target genes that are coregulated by ZHX2 and p65, including *IL6*, *IL8* (*CXCL8*), *CCL2*, *TNF*, *VCAM1* and *ICAM1* (Fig. 2c; Fig. S1)[33].

To confirm that Hippo pathway regulates NFκB signaling in ccRCC, we carried out RT-qPCR experiments to measure the change in NFκB target gene expression in ccRCC upon treatment with XMU-MP-1 at different doses or at a fixed concentration for increasing length of time. As shown in Fig. 2d, High dose of XMU-MP-1 resulted in a more dramatic downregulation of NFκB target gene expression. Similarly, increasing the duration of XMU-MP-1 treatment progressively decreased the expression of multiple NF-κB target genes without affecting the expression of p65 protein level (Fig. 2e; Fig. S2). These results suggest that XMU-MP-1 inhibits NFκB target gene expression in a dose- and time-dependent manner and that this downregulation is not due a change in the abundance of p65, a major subunit of NFκB in ccRCC[33]. Activation of YAP by the constitutively active YAP5SA resulted in inhibition of NF-κB target gene expression (Fig. 3a). On the contrary, knockdown of both YAP and TAZ using a previously validate siRNA[25,26], increased NFκB target gene expression (Fig. 3b). These results suggest that YAP negatively regulates NFκB signaling activity.

YAP regulates gene expression through the TEAD family of transcription factors including TEAD1-4[37]. RNAseq analysis revealed that TEAD1 and TEAD4 were more abundantly expressed than TEAD2 and TEAD3 in 786-O cells[26]. Overexpression of either TEAD1 or TEAD4 downregulated NF-κB target gene expression whereas knockdown of TEAD1/3/4 using previously validate siRNAs that targets shared sequences among these TEADs[12,25], led to increased expression of NF-κB target genes (Fig. 3c-d). These results supporting the notion that YAP acts in conjunction with TEAD to inhibit NFκB target gene expression.

YAP inhibits *ZHX2* expression

Analysis of the RNAseq data revealed that XMU-MP-1 treatment of 786-O cells also downregulated the expression of *ZHX2*. By RT-qPCR, we confirmed that MST1/2 inhibition by XMU-MP-1 decreased the expression of ZHX2 in 786-O cells (Fig. 2f). Expression of YAP-5SA

also downregulated whereas knockdown of YAP/TAZ increased *ZHX2* expression in 786-O cells (Fig. 3e-f), suggesting that YAP inhibits *ZHX2* expression.

Because ZHX2 is a critical cofactor for p65 in the regulation of NFκB target gene expression, YAP-mediated downregulation of ZHX2 could explain why XMU-MP-1 and YAP-5SA inhibit the expression of NFκB target genes. However, in time course experiments, we found that XMU-MP-1 inhibited NFκB target genes as well as *ZHX2* within 8 hours whereas ZHX2 protein levels were noticeably downregulated only after 16 hours treatment (Fig. S3a-c). Whereas transcriptional downregulation of *ZHX2* may contribute to a long-term shutdown of NFκB target gene expression by YAP activation, the immediate response of NF-κB target genes to XMU-MP-1 treatment is likely due to a differently mechanism(s).

YAP blocks the interaction between ZHX2 and p65

Because ZHX2 promotes NFκB target gene expression by physically interacting with p65, we carried out co-immunoprecipitation (Co-IP) experiments to determine whether YAP inhibits NFκB pathway activity by inhibiting p65/ZHX2 association. Using antibodies against endogenous proteins, we found that p65 formed a complex with ZHX2 as well as YAP and TEAD4 (Fig. 4a). Interestingly, XMU-MP-1 decreased the amount of ZHX2 associated with p65 while simultaneously increased the amount of YAP and TEAD4 bound to p65 (Fig. 4a), suggesting that YAP-TEAD may compete with ZHX2 for binding to p65.

To further characterize the competition between YAP-TEAD and ZHX2 for p65 binding, HEK293 cells were transfected with fixed amounts of Myc-tagged p65 (Myc-p65) and HA-tagged ZHX2 (HA-ZHX2) and increasing amounts of Flag-tagged YAP-5SA (Fg-YAP-5SA) or GFP-tagged TEAD4 (TEAD4-GFP), followed by Co-IP and western blot analysis. As shown in Fig. 4b, increasing the expression level of Fg-YAP-5SA progressively increased the amount of p65/Fg-YAP-5SA complex with concomitant decrease in the amount of p65-ZHX2 complex.

Furthermore, increasing the amount of Fg-YAP-5SA also resulted in an increase in the amount endogenous TEAD4 associated with Myc-p65. Similarly, increasing the amount of TEAD4-GFP led to a decrease in the amount of HA-ZHX2 associated with Myc-p65 but an increase in the amounts of TEAD4--GFP and endogenous YAP associated with Myc-p65. These results suggest that binding of YAP and TEAD to p65 disrupt the formation of the p65-ZHX2 complex. In a reciprocal experiment, HEK293 cells were transfected with fixed amounts of Myc-p65, Fg-YAP5SA and TEAD4-GFP, and increasing amount of HA-ZHX2. As shown in Fig. 4d, increasing the expression level of HA-ZHX2 progressively increased the amount of p65-ZHX2 complex with concomitant decrease in the amounts of Fg-YAP5SA and TEAD4-GFP associated with Myc-p65. Taken together, these results demonstrate that YAP-TEAD and ZHX2 compete for binding to p65.

YAP impedes binding of p65 and ZHX2 to NF-κB target promoters

ZHX2 and p65 co-occupy on the promoter/enhancer regions of many NFκB target genes and ZHX2/p65 interaction facilitates their promoter/enhancer occupancy to NF-κB target genes as knockdown of ZHX2 impaired p65 binding to *IL6* and *IKBKE* promoters, and vice versa[33]. Therefore, we tested whether YAP activation by Hippo pathway inhibition reduces the binding of p65/ZHX2 to the promoter regions of their coregulated genes by carrying ChIP-qPCR experiments. As shown in Fig. 5, after 786-O cells were treated with XMU-MP-1, both ZHX2 and p65 exhibited decreased chromatin association at multiple NF-κB target promoters co-bound by p65 and ZHX2, including *IL6*, *IL8*, and *CCL2* (Fig. 5a-c). Interestingly, p65 and ZHX2 co-occupy the promoter region of *ZHX2*, and their chromatin association was reduced by XMU-MP-1 treatment (Fig. 5a-c), suggesting that *ZHX2* is an autoregulated NF-κB target gene and that YAP inhibits *ZHX2* expression by disrupting p65/ZHX2 interaction.

ZHX2/p65 overexpression rescued ccRCC growth inhibited by XMU-MP-1

If Yap activation inhibits ccRCC cancer cell growth in 2D cultures by impeding p65/ZHX2 cooperativity, one would predict that increasing the activity of either ZHX2 or p65 may rescue ccRCC cancer cell growth inhibited by XMU-MP-1. To test this possibility, we overexpressed ZHX2 or p65 in 786-O cells via lentiviral infection and measure cancer cell growth in 2D cultures as well as NF-κB target gene expression in the absence or presence of XMU-MP-1 treatment. As expected, overexpression of either ZHX2 or p65 increased NF-κB target gene expression and promoted ccRCC cell growth in the absence of drug treatment (Fig. 6a-f). Importantly, ZHX2 or p65 overexpression significantly rescued ccRCC cell growth and NF-κB target gene expression after XMU-MP-1 treatment (Fig. 6a-f), lending further support that YAP inhibits ccRCC cancer cell growth by opposing the cooperative activity of p65 and ZHX2.

Discussion

Despite the prevailing view that Hippo signaling inhibits tumor growth by blocking the oncogenic potential of YAP/TAZ [2,14], recent studies revealed that YAP can act as a context-dependent tumor suppressor in several types of cancer [21-26,38,39]. Our previous study uncovered a noncanonical Hippo signaling mechanism in ccRCC whereby TEAD functions as a critical cofactor for the ccRCC oncogenic driver HIF-2α whereas nuclear YAP inhibits HIF-2α signaling by competing with HIF-2α for TEAD[26]. Analogous mechanisms have also been proposed to account for the tumor suppressor function of YAP in ERα^+ breast cancer and AR$^+$ prostate cancer[23 25]. In the current study, we uncovered yet another mechanism by which YAP inhibits cancer cell growth, i.e., through inhibiting the NFκB signaling pathway.

Previous studies showed that the growth of *VHL*$^{-/-}$ ccRCC cancer cells in 2D cultures was independent of HIF-2α activity[31,35,36]. Our observation that XMU-MP-1 could inhibit *VHL*$^{-/-}$ ccRCC growth not only in soft agar (3D culture) but also in 2D culture, a condition in which HIF-2α is

dispensable for 786-O growth, implied that YAP may inhibit *VHL*$^{-/-}$ ccRCC growth through additional mechanism(s) independent of HIF-2α. Furthermore, such inhibitory mechanism depends on the status of VHL as restoring VHL activity in 786-O cells blunted the inhibitory effect of XMU-MP-1, suggesting that YAP may inhibit 786-O cell growth through another VHL substrate(s). The recent finding that ZHX2 is a VHL substrate that promotes ccRCC cancer progression by forming a complex with p65 to regulate NF-κB target genes let us to speculate that YAP may target the p65-ZHX2 signaling axis. Indeed, we found that treatment of 786-O with XMU-MP-1 downregulated many NF-κB target genes coregulated by p65 and ZHX2 (Fig. S1). XMU-MP-1 treatment disrupted the interaction between p65 and ZHX2 while increasing the interaction between p65 and YAP/TEAD. Co-IP experiments in a heterologous system further demonstrate the competition between YAP/TEAD and ZHX2 for p65 binding. Increasing the activity of ZHX2/p65 largely rescued ccRCC growth inhibited by XMU-MP-1. Based on these and other observations, we propose that YAP inhibits NF-κB signaling in ccRCC by opposing p65/ZHx2 cooperativity, which contributes to ccRCC growth inhibition (Fig. 7).

ccRCC is responsible for most of the kidney cancer-associated death. Therapies targeting HIF-2α downstream effectors such as VEGF are the standard of care; however, drug resistance occurs in most patients[32,40]. HIF-2α inhibitors have recently entered the clinic; however, ccRCC patient samples exhibited differential sensitivity to HIF-2α inhibitors and HIF-2α mutants could render drug resistance[30,41]. Our findings that Hippo pathway inhibition or YAP activation not only inhibits HIF2α but also NF-κB signaling in ccRCC open a possibility for developing novel therapeutics to treat ccRCC.

Materials and Methods

DNA constructs

Myc-p65, HA-ZHX2, TEAD4-GFP, VHL, TAZ4SA and Flag-YAP were amplified by PCR and the products were sub-cloned to pLVX-zsGreen vector. The Flag-MST2-wt were amplified by PCR. To generate Flag-MST2-dm, Y101F/D109A double mutation was amplified by PCR-based mutagenesis from Flag-MST2 and the product was subcloned to pLVX-ZsGreen vector. The YAP-WT and YAP-5SA constructs were described previously[42]. YAP-WT or YAP-5SA were cloned into the pLVX-IRES-ZsGreen vector. GFP and YAP5SA coding sequences were subclone into pTet-O-Ngn2-puro (Addgene plasmid, Cat. No 52047) to generate Tet-O-GFP and Tet-O-YAP5SA. pLenti CMV rtTA3 Hygro (Addgene plasmid, Cat. No. 26730) was used to generate Dox-inducible cell lines.

Cell cultures

786-O, A498 and RCC4 are maintained with RPMI-1640 (Gibco, Cat. No. 42401018) supplemented with 2 mM L-glutamine (Gibco, Cat. No. 25030081) and 10% FBS. The HEK293A and HEK293T cells are culture with high glucose Dulbecco's Modified Eagle's Medium that contains 4.5 g/L glucose and 4 mM L-glutamine (DMEM, Gibco, Cat. No. 11965092) supplemented with 10% Fetal Bovine Serum (FBS, Gibco, Cat. No. 16000044).

Immunoblot analysis

Cells were harvested and lysed with lysis buffer containing 1M Tris pH8.0, 5M NaCl, 1M NaF, 0.1M Na_3VO_4, 1% NP-40, 10% glycerol, and 0.5M EDTA (pH 8.0). Proteins were separated by electrophoresis on SDS-polyacrylamide gel electrophoresis (PAGE) and electro-transferred to PVDF membrane. Membranes were washed with TBST and incubated with primary antibodies for 2 hours. And then the membranes were washed for three times with TBST and incubated

with second antibodies for 2 hours, after washed for three times with TBST, the membranes were probed with ECL system (Cytiva, Cat. No. RPN2105). The antibodies used in this study were listed here: rabbit anti-p65 (Cell Signaling Technology Cat.No,8242); rabbit anti-ZHX2 (Genetex, Cat.No. 112232); mouse anti-H3 (Santa Cruz, Cat. No. sc-517576); mouse anti-tubulin (Santa Cruz, Cat. No. sc-5288) ; mouse anti-GAPDH (Santa Cruz, Cat. No. sc-47724); mouse anti-YAP (Santa Cruz, Cat. No. sc-101199); mouse anti-TEAD4 (Santa Cruz, Cat. No. sc-101184); rabbit anti-HA (COVANCE, Cat. No. MMS-101R); mouse anti-Myc (Santa Cruz, Cat.No.SC-40); anti-Flag (Sigma, Cat. No. F3165); anti-GFP (Abcam, Cat. No. ab290). Peroxidase-Conjugated AffiniPure Goat Anti-Mouse IgG (Jackson ImmunoResearch, Cat.No. 115-035-003) or Goat Anti-Rabbit IgG (Jackson ImmunoResearch, Cat.No.111-035-144). Chemiluminescent signals were visualized with ECL system (Cytiva, Cat. No. RPN2105).

Co-immunoprecipitation assay

Immunoprecipitation was performed according to standard protocol. 786-O cell lysates were incubated with antibodies or mouse IgG for overnight at 4℃, followed by immobilization and precipitation with Protein A resin (Thermo Scientific Cat.No53139). The bound proteins were analyzed by western blot. For overexpression experiments, HEK293A cells were transfected with 5μg myc-p65, HA-ZHX2, Flag-YAP and GFP-TEAD4 plasmids in 10 cm dishes. Cell lysates were incubated with antibodies against epitope tags for overnight, followed by immobilization and precipitation with Protein A resin. The bound proteins were analyzed by immunoblot assay. Antibodies used for IP experiments: anti-p65 (Cell Signaling Technology Cat.No,8242), anti-ZHX2 (Genetex, Cat.No. 112232), anti-YAP (Santa Cruz, Cat. No. SC-101199), anti-TEAD4 (Santa Cruz, Cat. No. sc-101184), anti-Flag (Sigma, Cat.No. F3165), anti-Myc (Santa Cruz, Cat.No.SC-40), anti-GFP (Abcam, Cat. No. ab290), or mouse IgG (Santa Cruz, Cat.No. SC-3881).

RNA interference

For RNAi experiments in renal cancer cells, the siRNAs were acquired from the Sigma-Aldrich. The RNAi MAX reagent (Invitrogen Cat. No. 13778150) was used for the transfection of siRNA according the manuscription. Knockdown efficiency was validated by RT-PCR and/or immuno-blotting. The sequences for YAP/TAZ silencing were: 5'-UGU GGA UGA GAU GGA UA CA-3' and 5'-UGT AUC CAU CUC AUC CAC A-3'. The sequences for TEAD1/3/4 silencing were: 5'-AUG AUC AAC UUCA UCC ACA AG -3' and 5' GAU CAA CUU CAU CCA CAA GCU -3'. The sequences for negative control were: 5'-UUC UCC GAA CGU GUC ACG U-3'.

Virus infection and transient transfection

For packaging lentivirus, HEK293T cells were transfected with the expression vectors and package vectors (psPAX2 and pMD2.G) by PolyJet (SignaGen laboratories, Cat. No. SL100688). After 48 hours, the supernatants of the medium were collected and filtered with 0.45 μm filter. The supernatant containing virus was stored in 4℃ for cell infection. The ccRCC cells were cultured in fresh media and subsequently infected with lentivirus overnight together with Polybrene (Sigma, Cat. No. H9268). Hygromycin B (Sigma, Cat. No. 10843555001) and Puromycin (Sigma, Cat. No. P9620) were used for infected cells selection according to the resistance of the vectors.

RNA extraction and RT-qPCR analysis

We extracted the total RNA by RNeasy plus mini kits according to the protocol (Qiagen, Cat. No. 74106). After RNA extraction, the RNA was subjected to reverse transcription PCR for cDNA synthesis according to the RT-PCR kit (Applied Biosystems, Cat. No. 4368814). The relative gene expression was measured according to $2^{-\Delta\Delta CT}$ methods. The house keeping gene 36B4 was used for internal control. The Primer sequences were: 36B4, F: GGC GAC CTG GAA GTC CAA CT; R: CCA TCA GCA CCA CAG CCT TC;IL6, F: AGA CAG CCA CTC ACC TCT

TCA G, R: TTC TGC CAG TGC CTT TTG CTG; IL8, F: GAG AGT GAT TGA GAG TGG ACC AC, R: CAC AAC CCT CTG CAC CCG ATT T; TNF, F: CTC TTC TGC CTG CTG CAC TTT G; R: ATG GGC TAC AGG CTT GTC ACT C; CCL2, F: AGA ATC ACC AGC AGC AAG TGT CC, R: TCC TGA ACC CAC TTC TGC TTG G; ICAM1, F: AGC GGC TGA CGT GTG CAG TAA T, R: TCT GAG ACC TCT GGC TTC GTC A; VCAM1, F: GAT TCT GTG CCC ACA GTA AGG C, R: TGG TCA CAG AGC CAC CTT CTT G; ZHX2, F: ACA CGG GAC CGA TAT GAT GC, R: TTG GAG GGG GAT AAG GAG GG.

ChIP qPCR

ChIP (Chromatin Immuno-precipitation) assay was performed as previously study description[43], In brief, cells were cross-linked using 2 mM DSG crosslinker (CovaChem, Cat. No.13301) at room temperature for 1 h, followed by secondary fixation with 1% formaldehyde (Pierce, Cat. No. 28908) for 10 min and quenched by glycine. Subsequently, cells were washed with cold PBS and subject to cell lysis. The cell extracts were sonicated by Bioruptor. After centrifuge, the supernatants were incubated with prepared p65/ZHX2/TEAD4 antibody-Dynabeads for 1 hour room temperature and another 1 hour at 4℃. The slurries were washed in wash buffer for 5 times and de-cross-linked ChIP in elution buffer at 65℃ overnight. The enriched DNA was extracted via DNA extraction kits (Qiagen, Cat. No. 28106) and subject to quantitative PCR analysis. The Primer sequences for ChIP-qPCR were: IL6, F: CTT CGT GCA TGA CTT CAG CTT T, R: AGG GGG AAA AGT GCA GCT TAG; IL8, F: TTC CAC ACA TGG TCA AGG GG, R: CCT TCT CCA GGC TCC ATT CA; ZHX2, F: ATT GCA CGG AGA CGG TTT GG, R: ACG GAC TCG GTG GAA TTT CT; CCL2, F: TTG TGC CGA GAT GTT CCC AG, R: TGG CGT GAG AGA AGT GAG TG. The antibodies used in ChIP-qPCR were anti-p65 (Cell Signaling Technology Cat.No,8242), anti-TEAD4 (Santa Cruz, Cat. No. SC-101184) and anti-ZHX2 (Genetex, Cat.No. 112232). Anti-rabbit IgG dynabeads (Invitrogen, Cat: 11204D) and anti-mouse IgG dynabeads (Invitrogen, Cat. No. 11031) were used to bind antibodies.

RNA sequencing and data analysis

The global gene expression analysis (Vehicle vs XMU-MP-1 treated groups) was based on RNA sequencing platform from BGI (Beijing Genomic Institute). Cellular RNA was extracted using Qiagen RNA extraction kit (Qiagen; Cat: 74104) according to the manufacturer's instructions. The cellular RNA was sent to BGI Genomics (https://www.bgi.com) for RNA sequencing. RNA was quality-accessed with an Agilent 2100 Bioanalyzer (Agilent RNA 6000 Nano Kit) with RNA integrity number above 9 for library construction. The total RNA was used for library construction according to the protocol of BGISEQ-500 platform. The libraries were sequenced using BGISEQ-500 platform. Then the FASTQ sequencing files were aligned to the hg19 human genome using STAR aligner with uniquely mapped reads kept for further analysis. Differential expression was analyzed using DESeq2 with default parameters. The RNA sequence data are deposited in the Gene Expression Omnibus (GEO) database (Assessing number: GSE197468). For gene set enrichment analysis of RNA-seq data, gene sets of HIF2A activated target genes was used and downloaded from Molecular Signatures Database v7.4, GSEA was implemented using the GSEA 4.1.0 software, with default parameters. Volcano plot of DEGs (Threshold $P<0.01$ and fold change>2) was generated using the OmicStudio tools (https://www.omicstudio.cn/tool).

Statistics and reproducibility

All experiments were performed at least three independent times unless noted. Student's t-test was used for comparisons. A P-value of < 0.05 was considered to be significant. Error bars on the graphs were presented as the s.d.

Acknowledgements

We thank Drs. James Brugarolas and Qing Zhang for providing ccRCC cell lines. The work was supported by grants from NIH to JJ (R35GM118063, P50CA196516) and YY (R01CA222571), and

Welch foundation (I-1603) to JJ.

Author contributions

X.L., Y.C., S.Z., performed the experiments. X.L., Y.S., Y.L., Y.Y, S.Z., J.J. analyzed the data, X.L., S.Z., and J.J. designed the experiments. X.L. and J.J. wrote the manuscript.

Competing financial interests

The authors declare no competing financial interests.

Reference

1 Zhang, L., Yue, T. & Jiang, J. Hippo signaling pathway and organ size control. *Fly* **3**, 68-73 (2009).

2 Yu, F. X., Zhao, B. & Guan, K. L. Hippo Pathway in Organ Size Control, Tissue Homeostasis, and Cancer. *Cell* **163**, 811-828 (2015). https://doi.org:10.1016/j.cell.2015.10.044

3 Zheng, Y. & Pan, D. The Hippo Signaling Pathway in Development and Disease. *Dev Cell* **50**, 264-282 (2019). https://doi.org:10.1016/j.devcel.2019.06.003

4 Wu, S., Huang, J., Dong, J. & Pan, D. hippo encodes a Ste-20 family protein kinase that restricts cell proliferation and promotes apoptosis in conjunction with salvador and warts. *Cell* **114**, 445-456 (2003).

5 Harvey, K. F., Pfleger, C. M. & Hariharan, I. K. The Drosophila Mst ortholog, hippo, restricts growth and cell proliferation and promotes apoptosis. *Cell* **114**, 457-467 (2003).

6 Pantalacci, S., Tapon, N. & Leopold, P. The Salvador partner Hippo promotes apoptosis and cell-cycle exit in Drosophila. *Nat Cell Biol* **5**, 921-927 (2003).

7 Jia, J., Zhang, W., Wang, B., Trinko, R. & Jiang, J. The Drosophila Ste20 family kinase dMST functions as a tumor suppressor by restricting cell proliferation and promoting apoptosis. *Genes Dev* **17**, 2514-2519 (2003).

8 Udan, R. S., Kango-Singh, M., Nolo, R., Tao, C. & Halder, G. Hippo promotes proliferation arrest and apoptosis in the Salvador/Warts pathway. *Nat Cell Biol* **5**, 914-920 (2003). https://doi.org:10.1038/ncb1050

9 Zhao, B. *et al.* Inactivation of YAP oncoprotein by the Hippo pathway is involved in cell contact inhibition and tissue growth control. *Genes Dev* **21**, 2747-2761 (2007).

10 Dong, J. *et al.* Elucidation of a universal size-control mechanism in Drosophila and mammals. *Cell* **130**, 1120-1133 (2007).

11 Zhang, L. *et al.* The TEAD/TEF family of transcription factor Scalloped mediates Hippo signaling in organ size control. *Dev Cell* **14**, 377-387 (2008).

12 Zhao, B. *et al.* TEAD mediates YAP-dependent gene induction and growth control. *Genes Dev* **22**, 1962-1971 (2008). https://doi.org:10.1101/gad.1664408

13 Wu, S., Liu, Y., Zheng, Y., Dong, J. & Pan, D. The TEAD/TEF family protein Scalloped mediates transcriptional output of the Hippo growth-regulatory pathway. *Dev Cell* **14**, 388-398 (2008). https://doi.org:S1534-5807(08)00035-X [pii]10.1016/j.devcel.2008.01.007

14 Zanconato, F., Cordenonsi, M. & Piccolo, S. YAP/TAZ at the Roots of Cancer. *Cancer Cell* **29**, 783-803 (2016). https://doi.org:10.1016/j.ccell.2016.05.005

15 Zhou, D. *et al.* Mst1 and Mst2 maintain hepatocyte quiescence and suppress hepatocellular carcinoma development through inactivation of the Yap1 oncogene. *Cancer Cell* **16**, 425-438 (2009). https://doi.org:10.1016/j.ccr.2009.09.026

16 Song, H. *et al.* Mammalian Mst1 and Mst2 kinases play essential roles in organ size control and tumor suppression. *Proc Natl Acad Sci U S A* **107**, 1431-1436 (2010). https://doi.org:0911409107 [pii]10.1073/pnas.0911409107

17 Camargo, F. D. *et al.* YAP1 increases organ size and expands undifferentiated progenitor cells. *Curr Biol* **17**, 2054-2060 (2007). https://doi.org:10.1016/j.cub.2007.10.039

18 Lee, K. P. *et al.* The Hippo-Salvador pathway restrains hepatic oval cell proliferation, liver size, and liver tumorigenesis. *Proceedings of the National Academy of Sciences of*

the United States of America **107**, 8248-8253 (2010). https://doi.org:10.1073/pnas.0912203107
19 Lu, L. *et al.* Hippo signaling is a potent in vivo growth and tumor suppressor pathway in the mammalian liver. *Proc Natl Acad Sci U S A* **107**, 1437-1442 (2010). https://doi.org:0911427107 [pii]0.1073/pnas.0911427107
20 Zhang, N. *et al.* The Merlin/NF2 tumor suppressor functions through the YAP oncoprotein to regulate tissue homeostasis in mammals. *Dev Cell* **19**, 27-38 (2010). https://doi.org:S1534-5807(10)00305-9 [pii]10.1016/j.devcel.2010.06.015
21 Cottini, F. *et al.* Rescue of Hippo coactivator YAP1 triggers DNA damage-induced apoptosis in hematological cancers. *Nature medicine* **20**, 599-606 (2014). https://doi.org:10.1038/nm.3562
22 Ma, S. *et al.* Hippo signalling maintains ER expression and ER(+) breast cancer growth. *Nature.* **591**, E1-E10 (2021). https://doi.org:10.1038/s41586-020-03131-5
23 Li, X. *et al.* YAP inhibits ERalpha and ER(+) breast cancer growth by disrupting a TEAD-ERalpha signaling axis. *Nature communications* **13**, 3075 (2022). https://doi.org:10.1038/s41467-022-30831-5
24 Ma, S. *et al.* Transcriptional repression of estrogen receptor alpha by YAP reveals the Hippo pathway as therapeutic target for ER(+) breast cancer. *Nature communications* **13**, 1061 (2022). https://doi.org:10.1038/s41467-022-28691-0
25 Li, X. *et al.* YAP antagonizes TEAD-mediated AR signaling and prostate cancer growth. *Embo Journal.* **42**, e112184 (2023). https://doi.org:10.15252/embj.2022112184
26 Li, X., Cho, Y. S., Zhu, J., Zhuo, S. & Jiang, J. The Hippo pathway effector YAP inhibits HIF2 signaling and ccRCC tumor growth. *Cell Discov* **8**, 103 (2022). https://doi.org:10.1038/s41421-022-00465-4
27 Siegel, R. L., Miller, K. D. & Jemal, A. Cancer statistics, 2018. *CA Cancer J Clin* **68**, 7-30 (2018). https://doi.org:10.3322/caac.21442
28 Hsieh, J. J. *et al.* Renal cell carcinoma. *Nat Rev Dis Primers* **3**, 17009 (2017). https://doi.org:10.1038/nrdp.2017.9
29 Kondo, K., Klco, J., Nakamura, E., Lechpammer, M. & Kaelin, W. G., Jr. Inhibition of HIF is necessary for tumor suppression by the von Hippel-Lindau protein. *Cancer Cell* **1**, 237-246 (2002). https://doi.org:10.1016/s1535-6108(02)00043-0
30 Chen, W. *et al.* Targeting renal cell carcinoma with a HIF-2 antagonist. *Nature.* **539**, 112-117 (2016). https://doi.org:10.1038/nature19796
31 Cho, H. *et al.* On-target efficacy of a HIF-2alpha antagonist in preclinical kidney cancer models. *Nature.* **539**, 107-111 (2016). https://doi.org:10.1038/nature19795
32 Choueiri, T. K. & Kaelin, W. G., Jr. Targeting the HIF2-VEGF axis in renal cell carcinoma. *Nature medicine* **26**, 1519-1530 (2020). https://doi.org:10.1038/s41591-020-1093-z
33 Zhang, J. *et al.* VHL substrate transcription factor ZHX2 as an oncogenic driver in clear cell renal cell carcinoma. *Science* **361**, 290-295 (2018). https://doi.org:10.1126/science.aap8411
34 Fan, F. *et al.* Pharmacological targeting of kinases MST1 and MST2 augments tissue repair and regeneration. *Sci Transl Med* **8**, 352ra108 (2016). https://doi.org:10.1126/scitranslmed.aaf2304

35 Iliopoulos, O., Kibel, A., Gray, S. & Kaelin, W. G., Jr. Tumour suppression by the human von Hippel-Lindau gene product. *Nature medicine* **1**, 822-826 (1995). https://doi.org:10.1038/nm0895-822
36 Kondo, K., Kim, W. Y., Lechpammer, M. & Kaelin, W. G., Jr. Inhibition of HIF2alpha is sufficient to suppress pVHL-defective tumor growth. *PLoS biology* **1**, E83 (2003). https://doi.org:10.1371/journal.pbio.0000083
37 Currey, L., Thor, S. & Piper, M. TEAD family transcription factors in development and disease. *Development* **148** (2021). https://doi.org:10.1242/dev.196675
38 Li, Q. *et al.* Lats1/2 Sustain Intestinal Stem Cells and Wnt Activation through TEAD-Dependent and Independent Transcription. *Cell Stem Cell* **26**, 675-692 e678 (2020). https://doi.org:10.1016/j.stem.2020.03.002
39 Cheung, P. *et al.* Regenerative Reprogramming of the Intestinal Stem Cell State via Hippo Signaling Suppresses Metastatic Colorectal Cancer. *Cell Stem Cell* **27**, 590-604 e599 (2020). https://doi.org:10.1016/j.stem.2020.07.003
40 Escudier, B., Szczylik, C., Porta, C. & Gore, M. Treatment selection in metastatic renal cell carcinoma: expert consensus. *Nat Rev Clin Oncol* **9**, 327-337 (2012). https://doi.org:10.1038/nrclinonc.2012.59
41 Courtney, K. D. *et al.* HIF-2 Complex Dissociation, Target Inhibition, and Acquired Resistance with PT2385, a First-in-Class HIF-2 Inhibitor, in Patients with Clear Cell Renal Cell Carcinoma. *Clin Cancer Res* **26**, 793-803 (2020). https://doi.org:10.1158/1078-0432.CCR-19-1459
42 Cho, Y. S. *et al.* Regulation of Yki/Yap subcellular localization and Hpo signaling by a nuclear kinase PRP4K. *Nature communications* **9**, 1657 (2018). https://doi.org:10.1038/s41467-018-04090-2
43 Reddy, T. E. *et al.* Genomic determination of the glucocorticoid response reveals unexpected mechanisms of gene regulation. *Genome Res* **19**, 2163-2171 (2009). https://doi.org:10.1101/gr.097022.109

Xu_Fig1

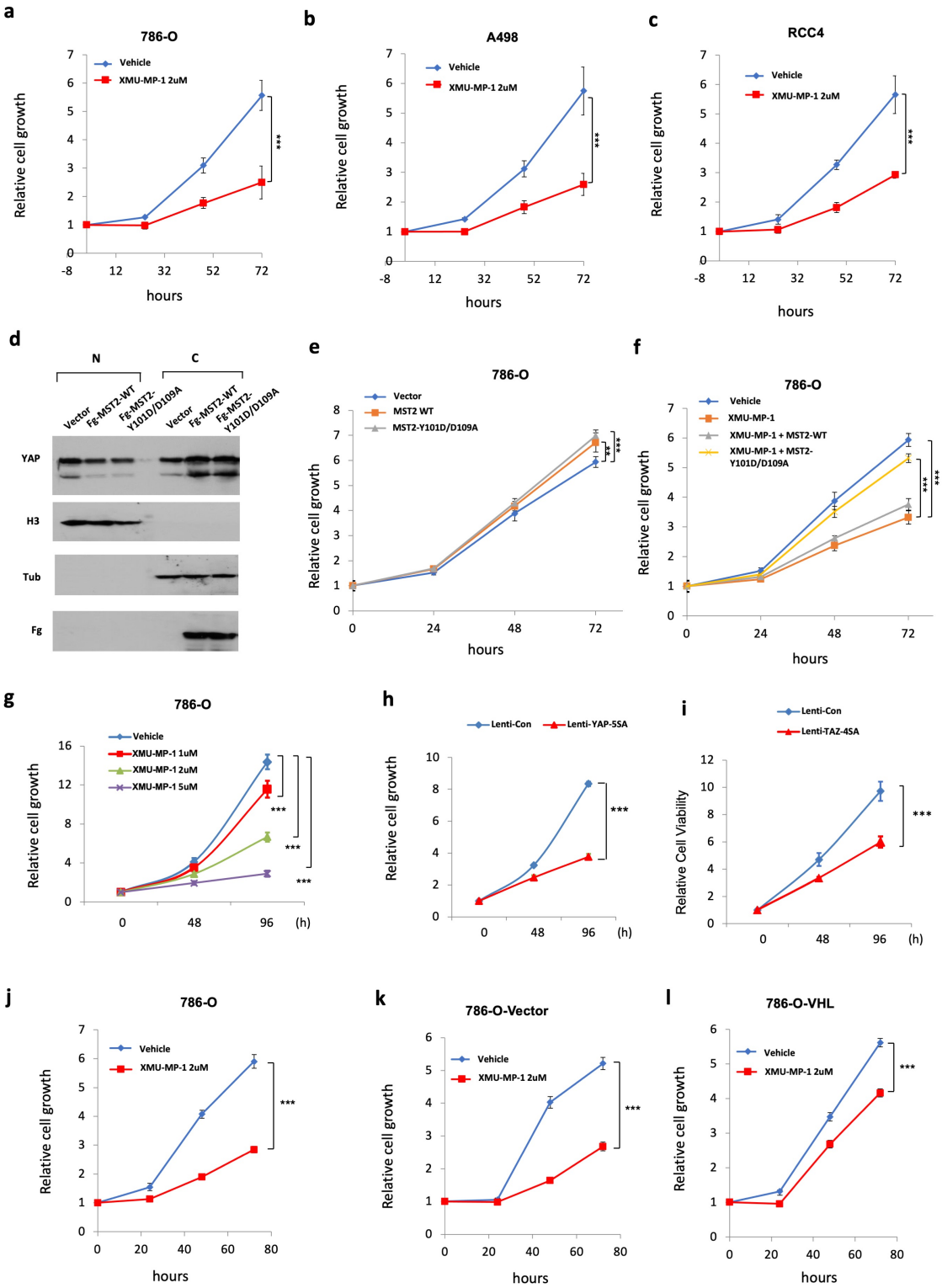
a
786-O
Vehicle
XMU-MP-1 2uM
Relative cell growth
hours
b
A498
c
RCC4
d
N
C
Vector
Fg-MST2-WT
Fg-MST2-Y101D/D109A
YAP
H3
Tub
Fg
e
786-O
Vector
MST2 WT
MST2-Y101D/D109A
f
XMU-MP-1
XMU-MP-1 + MST2-WT
XMU-MP-1 + MST2-Y101D/D109A
g
XMU-MP-1 1uM
XMU-MP-1 2uM
XMU-MP-1 5uM
(h)
h
Lenti-Con
Lenti-YAP-5SA
i
Lenti-TAZ-4SA
Relative Cell Viability
j
k
786-O-Vector
l
786-O-VHL

Figure 1 YAP activation inhibits ccRCC cancer cell growth in 2D cultures

a, b, c Growth of 786-O (**a**), A498 (**b**), and RCC4 (**c**) cells treated with vehicle or 2 μM XMU-MP-1. **d** Western blot analysis of nuclear (N) and cytoplasmic (C) fractions of 786-O cells expressing the indicated constructs. **e, f** Growth of 786-O cells expressing the indicated constructs in the absence (**e**) or presence (**f**) of XMU-MP-1 at 2 μM. **g** Growth of 786-O cells treated with increasing doses of XMU-MP-1. **h**, **i** Growth of 786-O cells expressing the indicated lentiviral constructs. **j, k, l** Growth of 786-O cells (**j)** and 786-O cells expressing an empty vector (**k**) or VHL (**l**) and treated with vehicle or 2 μM XMU-MP-1. Data are ± SD. $^{**}P<0.01$, $^{***}P<0.001$ (Student's t-test).

Xu_Fig2

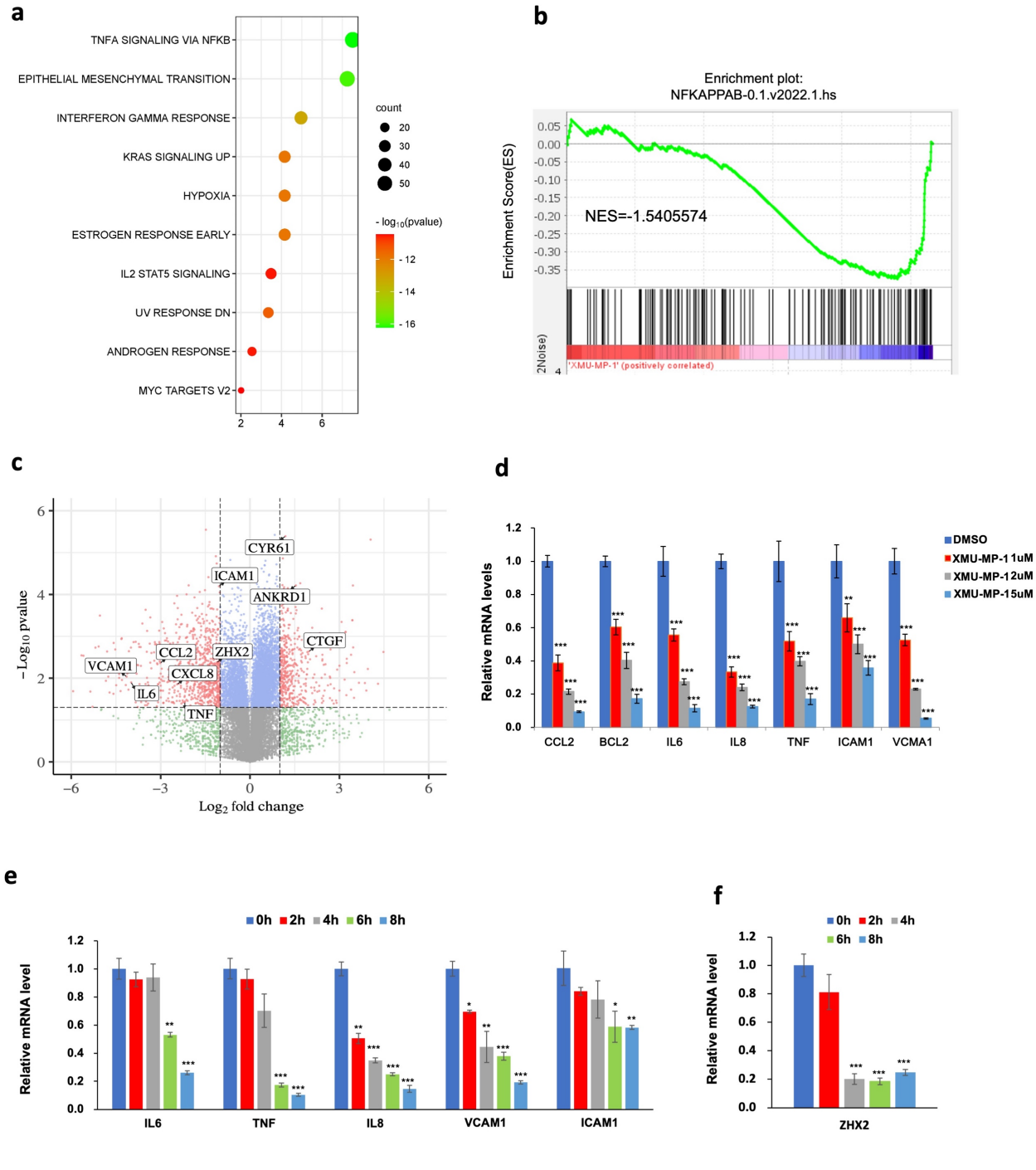
a
TNFA SIGNALING VIA NFKB
EPITHELIAL MESENCHYMAL TRANSITION
INTERFERON GAMMA RESPONSE
KRAS SIGNALING UP
HYPOXIA
ESTROGEN RESPONSE EARLY
IL2 STAT5 SIGNALING
UV RESPONSE DN
ANDROGEN RESPONSE
MYC TARGETS V2
count
20
30
40
50
- log10(pvalue)
- 12
- 14
- 16
b
Enrichment plot:
NFKAPPAB-0.1.v2022.1.hs
Enrichment Score(ES)
NES=-1.5405574
'XMU-MP-1' (positively correlated)
c
CYR61
ICAM1
ANKRD1
CTGF
CCL2
ZHX2
VCAM1
CXCL8
IL6
TNF
−Log10 pvalue
Log2 fold change
d
DMSO
XMU-MP-11uM
XMU-MP-12uM
XMU-MP-15uM
Relative mRNA levels
CCL2
BCL2
IL6
IL8
TNF
ICAM1
VCMA1
e
0h
2h
4h
6h
8h
Relative mRNA level
IL6
TNF
IL8
VCAM1
ICAM1
f
0h
2h
4h
6h
8h
Relative mRNA level
ZHX2

Figure 2 XMU-MP-1 inhibits NF-κB transcriptome in ccRCC

a Top 10 signaling pathways downregulated in 786-O cells treated with XMU-MP-1. **b** Gene set enrichment analysis (GSEA) shows downregulation of NF-κB target genes in 786-O cells treated with XMU-MP-1. **c** Volcano plot shows the opposite effects of XMU-MP-1 treatment on NF-κB target genes and the Hippo pathway signature in 786-O cells treated with XMU-MP-1. **d** Relative mRNA levels of the indicated NF-κB target genes in 786-O cells treated with the indicated concentrations of XMU-MP-1. **e** Relative mRNA levels of the indicated NF-κB target genes in 786-O cells treated with XMU-MP-1 for 0, 2, 4, 6, or 8 hours. **f** Relative mRNA levels of the ZHX2 in 786-O cells treated with XMU-MP-1 for the indicated time. Data in **d**, **e**, **f** are ± SD. $^{*}P<0.05$, $^{**}P<0.01$, $^{***}P<0.001$ (Student's t-test).

Xu_Fig3

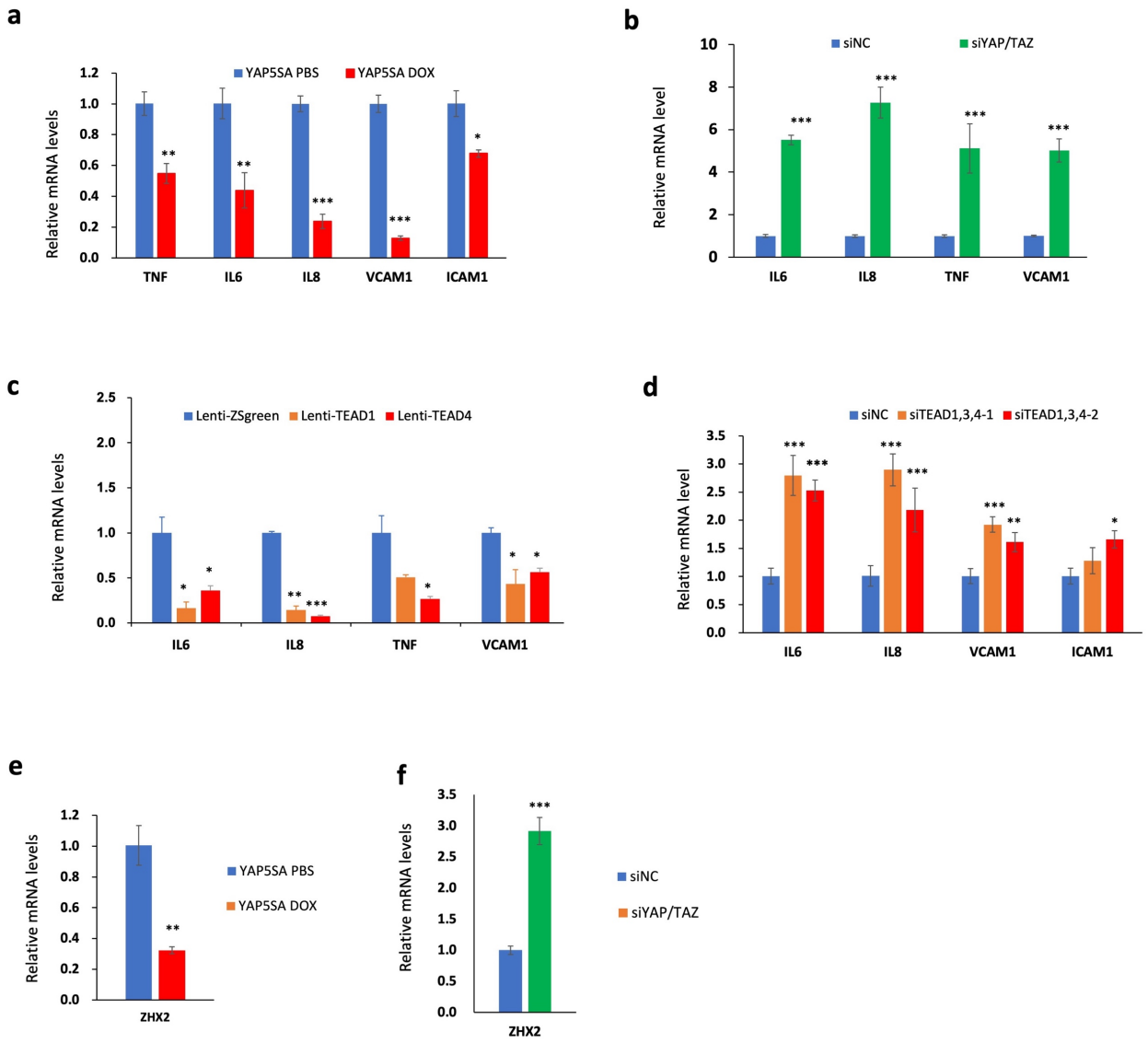

Figure 3 YAPTEAD inhibits NF-κB target gene expression in ccRCC

a Relative mRNA levels of the indicated NF-κB target genes in 786-O cells expressing Tet-O-YAP5SA and treated with PBS or Doxycycline (Dox). **b** Relative mRNA levels of the indicated NF-κB target genes in 786-O cells treated with control siRNA (siNC) or a siRNA targeting both

YAP and TAZ (siYAP/TAZ). **c** Relative mRNA levels of the indicated NF-κB target genes in 786-O cells infected with control, TEAD1 or TEAD4 lentivirus. **d** Relative mRNA levels of the indicated NF-κB target genes in 786-O cells treated with control siRNA or siRNAs targeting TEAD1/3/4. **e** Relative mRNA levels of *ZHX2* in 786-O cells expressing Tet-O-YAP5SA and treated with vehicle or Dox. **f** Relative mRNA levels of *ZHX2* in 786-O cells treated with siNC or siYAP/TAZ. Data are ± SD. $^{*}P<0.05$, $^{**}P<0.01$, $^{***}P<0.001$ (Student's t-test).

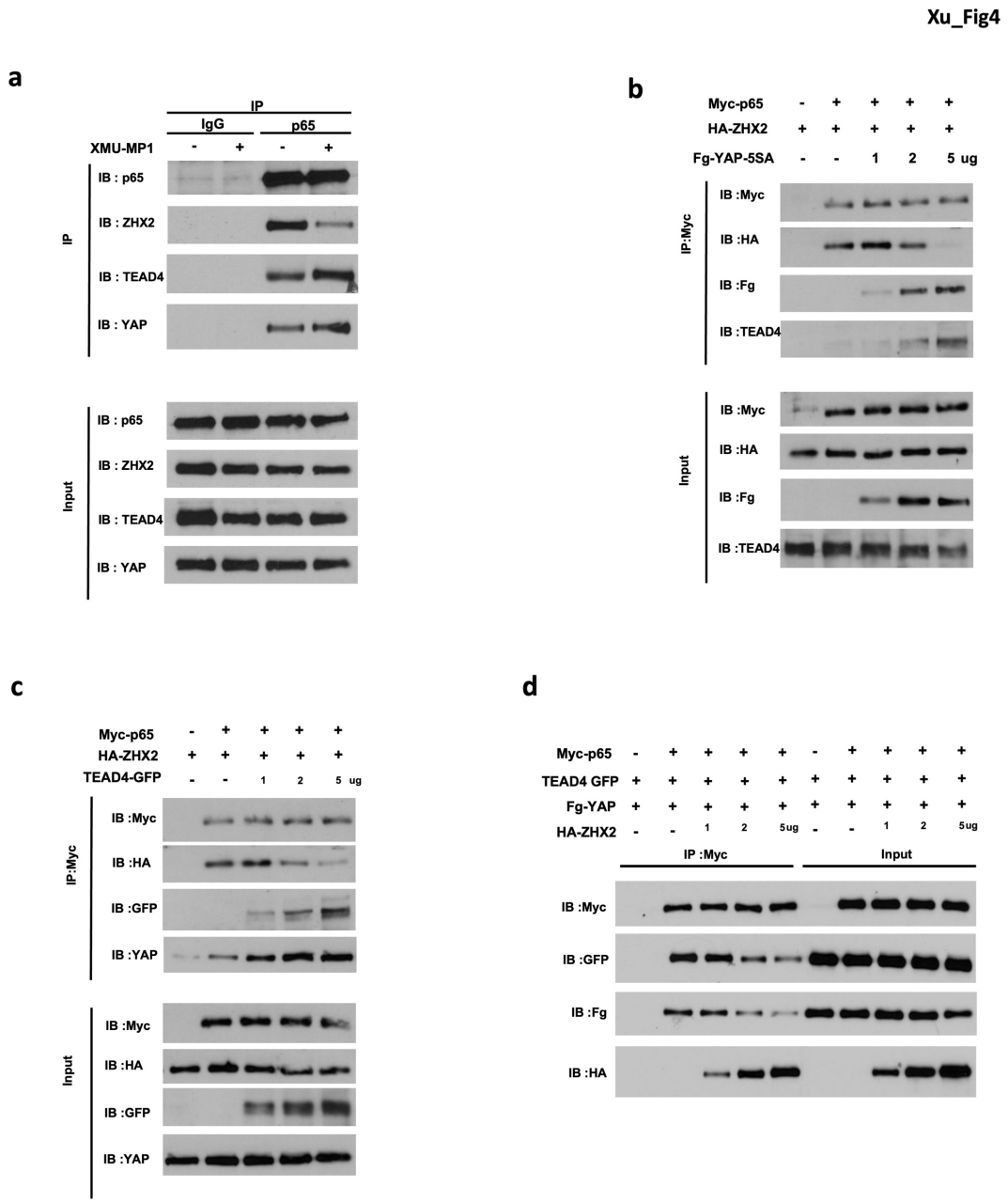

Figure 4 YAP/TEAD competes with ZHX2 for binding to p65

a Western blot analysis of endogenous p65, ZHX2, YAP and TEAD4 immunoprecipitated with control (IgG) or p65 antibody from cell extracts of 786-O cells grown without or with 2 μM XMU-MP-1 for 6 hours. **b, c** HEK293 cells were transfected with fixed amounts of Myc-p65 and HA-

ZHX-2 and increasing amounts of Fg-YAP-5SA (**b**) or TEAD4-GFP (**c**). Cell extracts were immunoprecipitated with an anti-Myc antibody, followed by western blot analysis with antibodies against the indicated tags, endogenous TEAD4 (**b**) or YAP (**c**). **d** HEK293 cells were transfected with fixed amounts of Myc-p65, Fg-YAP and TEAD4-GFP and increasing amounts of HA-ZHX-2. Cell extracts were immunoprecipitated with the anti-Myc antibody, followed by western blot analysis with antibodies against the indicated tags.

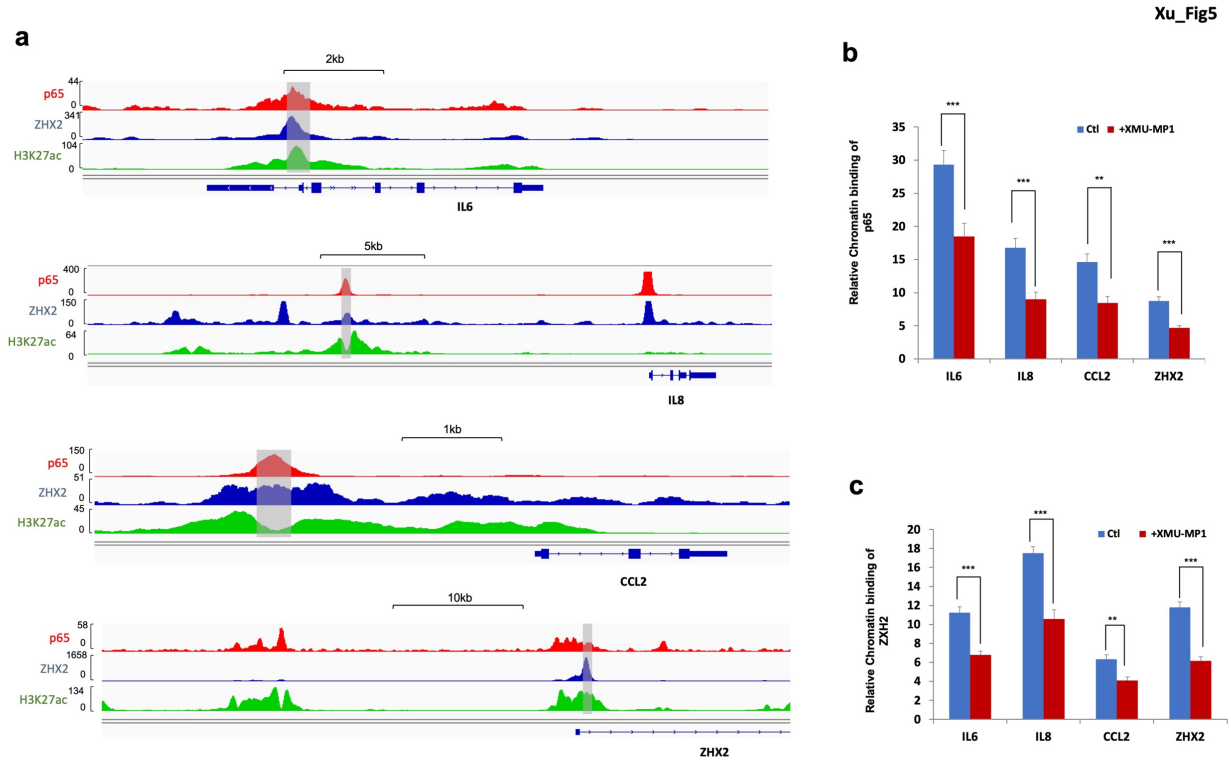

Figure 5 Hippo pathway inhibition impairs occupancy of p65 and ZXH2 on NF-κB target promoters

a Analysis of a published ChIP seq data indicates that p65 and ZHX2 co-bind sites in the promoter/enhancer regions of *IL6*, *IL8*, *CCL2* and *ZHX2* that are also enriched for H3K27ac.

b, c ChIP qPCR experiments show that treating 786-O cells with the Hippo pathway inhibitor XMU-MP-1 decreased the binding of p65 (**b**) and ZXH2 (**c**) to the promoter/enhancer regions (shaded regions in **a**) of *IL6*, *IL8*, *CCL2* and *ZXH2*. Data in are ± SD. **P<0.01, ***P<0.001 (Student's t-test).

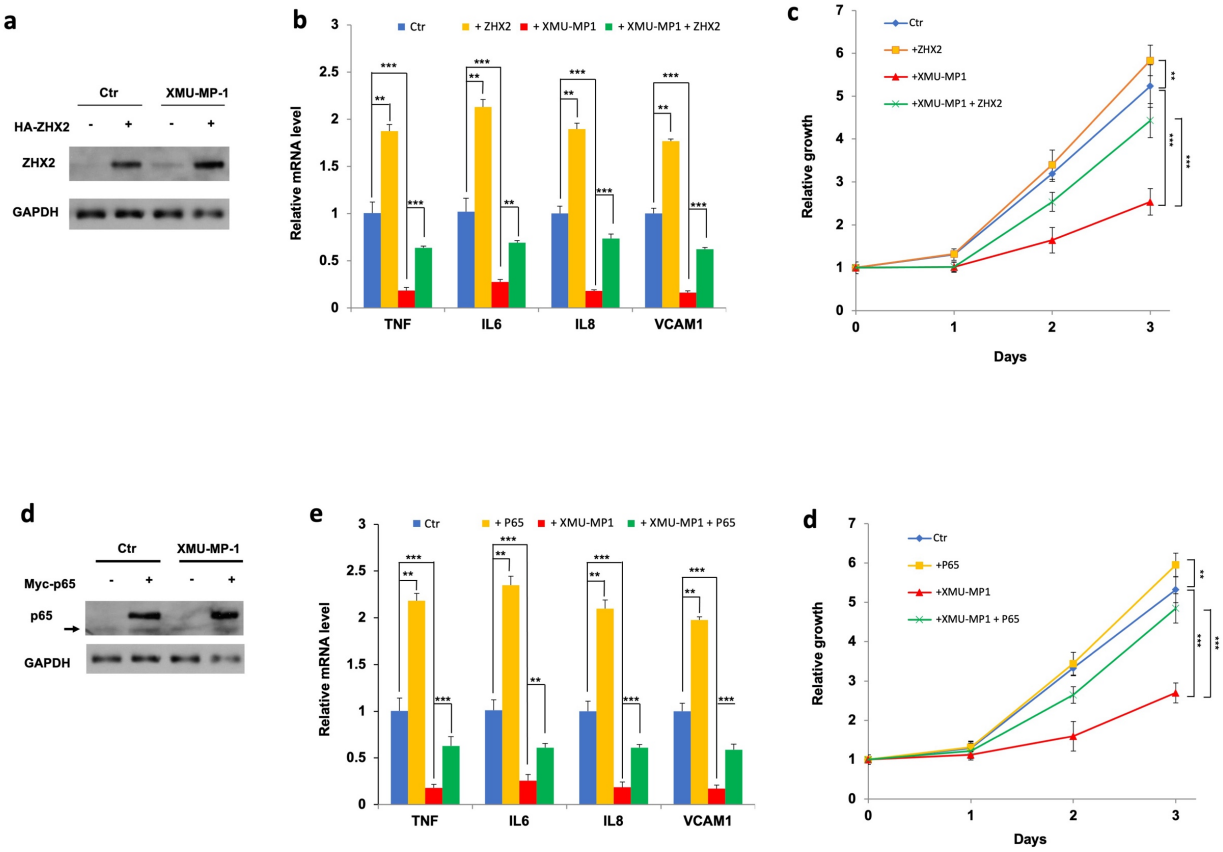

Figure 6 Increasing p65/ZHX2 activity rescues ccRCC growth inhibited by XMU-MP-1

a, **b** Western blot analysis of ZHX2 (**a**) and RT-qPCR analysis of the indicated NF-κB target gene expression (**b**) in 786-O cells infected with control or ZHX2 expressing lentivirus and treated with vehicles or 2 μM XMU-MP-1. Data in are ± SD. **P<0.01, ***P<0.001 (Student's t-test).

c Growth of 786-O cells infected with control or ZHX2 expressing lentivirus and treated with vehicles or 2 μM XMU-MP-1. Data in are ± SD. **P<0.01, ***P<0.001 (Student's t-test).

d, **e** Western blot analysis of p65 (**d**) and RT-qPCR analysis of the indicated NF-κB target gene expression (**e**) in 786-O cells infected with control or p65 expressing lentivirus and treated with

vehicles or 2 μM XMU-MP-1. Arrow in **d** indicates endogenous p65. Data in are ± SD. **P<0.01, ***P<0.001 (Student's t-test).

f Growth of 786-O cells infected with control or p65 expressing lentivirus and treated with vehicles or 2 μM XMU-MP-1. Data in are ± SD. **P<0.01, ***P<0.001 (Student's t-test).

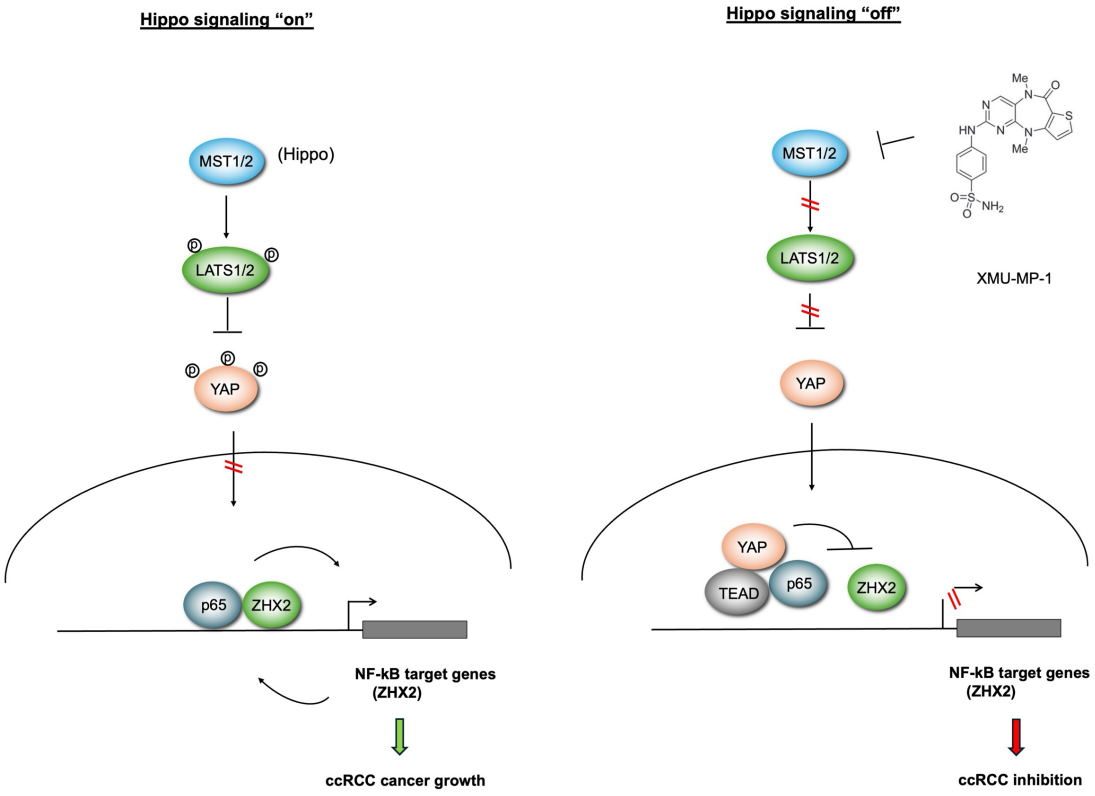

Figure 7 Hippo pathway inhibition impedes ccRCC growth by opposing p65/ZXH2 cooperativity

When Hippo signaling is "on", YAP is phosphorylated and excluded from the nucleus, allowing p65 and ZHX2 to cooperatively activate NF-κB target gene expression that drives ccRCC growth. When Hippo signaling is "off", YAP enters the nucleus and forms a complex with TEAD. YAP/TEAD impedes p65/ZHX2 cooperativity by disrupting their physical interaction, leading to downregulation of NF-κB target gene expression and growth inhibition.

Xu_FigS1

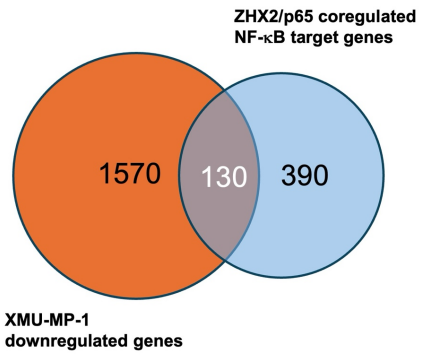

SCD	INSIG1	ABCC2	ABCC6	DSCAML1	VCAM1
CSF1	MEGF6	CARD6	IFIH1	IFI44L	CCL2
IRF9	C1orf106	HLX	MCTP1	RASSF9	VAV3
ABCA1	PTGER2	KY	NEFL	OLFML2B	CLEC4E
ZBTB38	CTHRC1	GRB7	TNFAIP3	ZHX2	CXCL8
SEC14L6	EPHB2	NID2	FOXP2	FRMD4B	C3
ZNF618	IFI44	BCL3	ARSE	IL1R1	KIF12
STEAP3	PER3	MAF	B3GNT4	CD24	TINAG
XAF1	ABLIM1	TLL1	TRIM22	STAT1	ITGB6
HGD	MRAS	MAML2	CNR1	SEMA3A	ENPP3
STAT6	MGLL	MSC	F8	HNF1B	ABCA12
C1QTNF6	IKBKE	DMRTA1	ACTR3C	FRK	SYNPO
PDZK1IP1	TNS1	TM4SF18	SLN	ARL14EPL	RNASET2
DDX60	LXN	SORCS2	OAS2	C1orf186	TMEM141
AHNAK2	ARHGEF6	TLR3	MMP1	CYP1B1	SEMA6A
PORCN	GCNT1	QPRT	FBXL13	SGPP2	SEMA5B
TNFSF10	DDX60L	SGK2	SLC44A3	OAS1	AGMO
TRIM38	BRINP1	PDGFB	PRKCQ	EFHB	TRABD2B
TNIP1	RYR3	SLC4A4	MAP7D2	SAA1	NCKAp5
RBPMS	MFNG	LIPG	GBP2	PLEK	TNFAIP6
ADAMTS9	IL6	PTGES	MTSS1	C14orf105	
TNS3	SHROOM4	MITF	SAMD9L	GPRC5B	

Fig. S1. XMU-MP-1 inhibits NF-κB target genes co-regulated by p65 and ZHX2

Overlap of XMU-MP1 downregulated genes and NF-kB target genes co-regulated by ZHX2 and p65 in 786-O cells (left). List of the 130 NF-kB target genes co-regulated by ZHX2 and p65 and downregulated by XMU-MP1 in 786-O cells (right).

Xu_FigS2

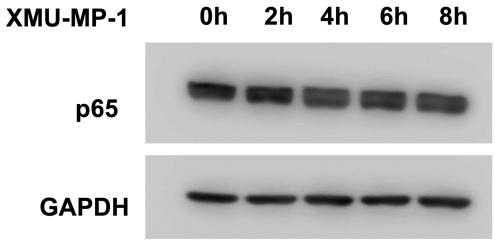

Fig. S2. Hippo pathway inhibition does not affect p65 protein level

Western blot analysis of p65 protein expression in 786-O cells treated with 2 μM XMU-MP-1 for the indicated time. GAPDH was used as a loading control.

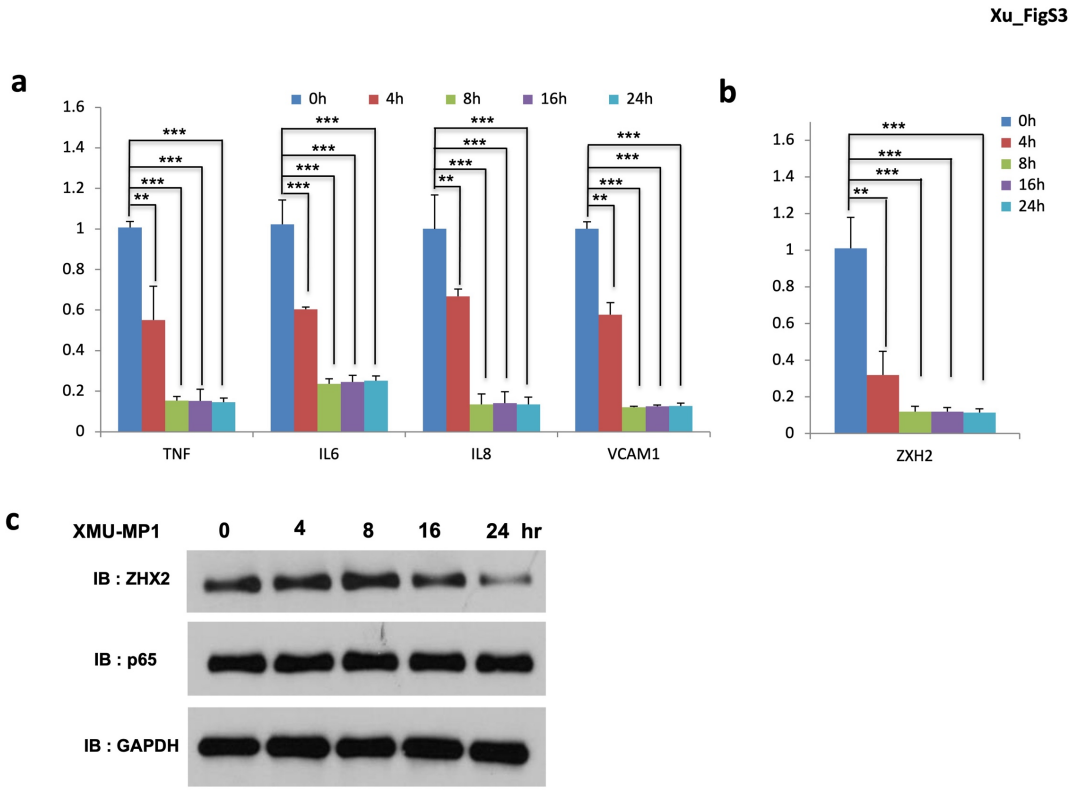

Fig. S3. XMU-MP-1 inhibits NF-κB target gene expression without affecting ZHX2 protein level

a, **b** Relative mRNA levels of the indicated NF-κB target genes (**a**) or *ZHX2* (**b**) in 786-O cells treated with 2 μM XMU-MP-1 for the indicated periods of time. Data in are ± SD. **P<0.01, ***P<0.001 (Student's t-test).

c Western blot analysis of ZHX2 and p65 protein expression in 786-O cells treated with 2 μM XMU-MP-1 for the indicated periods of time. GAPDH was used as a loading control. ZHX2 level started to decline after XMU-MP-1 treatment for 16 hours while p65 protein level remained unchanged even after 24 hours' treatment.